SAND2021-11136J

Achieving High Ethylene Yield in Non-Oxidative Ethane Dehydrogenation

Christopher Riley[a], Andrew De La Riva[b], Isabel Ibarra[b], Abhaya Datye[b,*], Stanley Chou[a,*]

[a] Sandia National Laboratories, Albuquerque, New Mexico, 87185, USA

[b] Department of Chemical and Biological Engineering and Center for Microengineered Materials, University of New Mexico, Albuquerque, New Mexico, 87131, USA

* Corresponding authors; datye@unm.edu; schou@sandia.gov

Abstract

Steam cracking of ethane, a non-catalytic thermochemical process, remains the dominant means of ethylene production. The severe reaction conditions and energy expenditure involved in this process incentivize the search for alternative reaction pathways and reactor designs which maximize ethylene yield while minimizing cost and energy input. Herein, we report a comparison of catalytic and non-catalytic non-oxidative dehydrogenation of ethane. We achieve ethylene yields as high as 68% with an open tube quartz reactor without the use of a catalyst at residence times ~4s. The open tube reactor design promotes simplicity, low cost, and negligible coke formation. Pristine quartz tubes were most effective, since coke formation was detected when defects were introduced by scratching the surface of the quartz. Surprisingly, the addition of solids to the quartz tube, such as quartz sand, alumina powder, or even Pt-based intermetallic catalysts, led to lower ethylene yield. Pt alloy catalysts are effective at lower temperatures, such as at 575 °C, but conversion is limited due to thermodynamic constraints. When operated at industrially relevant temperatures, such as 700 °C and above, these catalysts were not stable in our tests, causing ethylene yield to drop below that of the open tube. These results suggest that future research on non-oxidative dehydrogenation should be directed at optimizing reactor designs to improve the conversion of ethane to ethylene, since this approach shows promise for decentralized production of ethylene from natural gas deposits.

Key words: ethane dehydrogenation; non-oxidative; quartz reactor; ethylene yield; catalyst

Introduction

Industrial steam cracking of ethane and naptha is the dominant means of ethylene production, yielding over 150 million tons of ethylene per year globally. High production volume is required to meet the growing demand for ethylene, which serves as a crucial polymer and petrochemical precursor.[1] Although steam cracking operations are highly optimized, the process consumes significant energy (16 GJ/ton ethylene) and generates large quantities of CO_2 (approximately 1 ton CO_2/ton ethylene).[2] Steam cracking reactors are operated at extreme temperatures, typically between 850 – 950 °C, to raise the equilibrium conversion of ethane to ethylene, given the high endothermicity of this reaction.[3] Ethylene yield benchmarks are approximately 55%.[4] Co-fed steam reduces coke formation but adds significantly to the energy required to heat reactant streams and creates a corrosive environment within cracking reactors, lowering the lifespan of system components.[5] These severe operational conditions

fuel interest in developing alternative means of ethylene production, with focus placed on maximizing ethylene yield while minimizing energy input, operational costs, and capital investment. Decentralized production of ethylene from natural gas, which contains relatively dilute ethane concentrations (between 0 – 25%), is one potential approach. Such operations would require simplified reactor designs and milder operating conditions without sacrificing ethylene yield.

Because steam cracking is a noncatalytic thermochemical process, catalyzed reactions have received significant study as alternative means of ethylene production.[1] Catalyzed ethane dehydrogenation is a viable option, which can be performed under both oxidative and non-oxidative conditions. Co-feeding oxidizing agents, like O_2 or CO_2, lowers reaction endothermicity through creation of oxidized byproducts, like H_2O, mitigating thermodynamic constraints and allowing appreciable alkane conversion at lower reaction temperatures.[6-12] However, total oxidation of hydrocarbon reactants and formation of unwanted products is highly exothermic and thermodynamically favored. Catalytic oxidative dehydrogenation of ethane has achieved ethylene selectivity and yields better than steam cracking.[13] However, several studies do report excellent ethylene yield at the beginning of the reaction, followed by rapid deactivation.[6, 14, 15] A wide variety of molten salts[16, 17] and complex reducible oxide catalysts are studied for this reaction, which are based on chromia (as used industrially in the Catofin process),[6, 8-10, 15, 18] zirconia,[7, 14] niobia,[19-21] molybdenum,[22-25] and iron oxide constituents.[7, 26-29] Despite the significant cost, platinum-based catalysts are often chosen to facilitate non-oxidative dehydrogenation of ethane. Indeed, the industrial Olexflex process for dehydrogenation of propane utilizes Pt-Sn bimetallic catalysts.[30] Other Pt bimetallics have been investigated in the literature for ethane dehydrogenation with the general finding that alloying Pt reduces coke formation, increases ethylene selectivity, and improves Pt dispersion.[31-36] Compared to propane dehydrogenation, operational temperatures must be higher during ethane dehydrogenation to overcome increased reaction endothermicity. Previous studies tested Pt intermetallic catalysts within the temperature range of 500 – 750 °C, with varying degrees of catalyst deactivation observed.[32-37] Thus, the thermal stability of such catalysts applied in ethane dehydrogenation reaction is of particular concern.

The severe operational conditions involved in ethane dehydrogenation can be mitigated through novel reactor designs. Hydrogen-permeable membranes can increase equilibrium conversion of ethane. However, membranes add significantly to system cost,[38] and require a sweep gas,[39-41] which complicates system operation. Metallurgical improvements have allowed steel steam cracking furnace components to withstand higher operational temperatures, achieving high ethane conversion.[5] The influence of temperature, alloying elements, and co-fed steam have been thoroughly investigated to manage ethylene yield, coke formation, and reactor lifespan. Addition of nickel and niobium alloying elements to steel cracking furnaces improved thermal stability, but these inclusions promote coke formation and maintenance requirements.[5, 42] Accumulation of coke restricts gas flow within the furnace and leads to carburization of steels, which structurally degrades cracking furnace components. Alternative reactor wall materials and coatings made of alumina, silicon carbide, or quartz are proposed as potential replacements.[5, 43] Previous work shows that thermal reactions conducted in the gas phase are quite selective for the dehydrogenation of ethane to ethylene, because the activation barrier for the abstraction of a hydrogen atom from ethylene (461 KJ/mol) is higher than that for abstraction of hydrogen from ethane (410 KJ/mol).[44] On the contrary, olefins are much more reactive than alkanes on solid surfaces, and especially on Pt based catalysts, leading to coke formation. Hence, the

contribution of thermal reactions to ethane dehydrogenation at the lower temperatures where catalytic reactions are studied needs further investigation. Heracleous et al.[24] studied oxidative and non-oxidative dehydrogenation of ethane in an empty tube and with a 20 wt% Mo/Al_2O_3 catalyst. They reported that the presence of oxygen was beneficial for ethane conversion even for the homogeneous reaction carried out in an empty tube. A similar yield of ethylene was reported for oxidative dehydrogenation at 700 °C for the homogeneous and the catalyzed reaction (approximately 56% with a 2% ethane feed). For the non-oxidative dehydrogenation, they reported significant coke formation with a H_2/C_2H_4 ratio greater than 1 for the empty tube. On the other hand, Xu et al.[45] reported excellent selectivity to ethylene in an empty quartz tube reactor at 700 °C. Some of these differences in coke formation and selectivity may be a result of the reactor wall composition and the influence of the solid phase (catalyst or catalyst support). Thus, a comparative study which varies reactor materials and design, operated with and without a catalyst, is needed.

Here, we compare the catalyzed and non-catalyzed non-oxidative dehydrogenation of ethane. We explored various reactor configurations, including open tube, annular, and packed bed reactors. Reactor tube materials studied were quartz, alumina, and stainless-steel. Packed beds of state-of-the-art Pt-based catalysts, as well as inert materials, were also studied. We demonstrate that an open tube reactor design can convert ethane to ethylene with high yields without addition of a catalyst or co-fed steam or H_2, meeting or exceeding benchmarks from steam cracking. Using a feed consisting of 2.5 - 25% ethane in nitrogen (consistent with ethane concentrations in natural gas deposits), we achieve a yield of 68% at a maximum reactor temperature near 750 °C. Careful preparation of reactor walls allows for negligible coke formation. Without the use of a catalyst or concern for coke formation, the open tube reactor demonstrates stable performance without any deactivation or the need for regeneration. The quartz tube reactor is not prone to carburization, which degrades conventional cracking furnace components. We find that Pt-based catalysts are effective at low temperatures, such as 600 °C. However, the performance of these catalysts deteriorates when operated at temperatures of 700 °C and higher. The simplicity of the open tube quartz reactor suggests that further research on novel designs that quench the products and allow better heat integration might provide an alternative to the capital-intensive steam cracking process for distributed manufacturing of ethylene from shale gas.

Materials and Methods

Multiple reactor configurations were tested to evaluate ethane dehydrogenation reactivity, including open-tube, annular, and packed beds containing catalysts as well as inert materials. Inert materials were tested to determine any beneficial effects in terms of initiating thermochemically-induced free radical reactions and low activity for ethylene hydrogenation or undesired coke formation at high temperatures, which may lower the yield. The reactor tubes were made of fused silica quartz (4 mm ID and 6 mm OD, Technical Glass Products, Inc.), 316L stainless-steel (3.5 mm ID and 6.35 mm OD, Swagelok), and alumina (4.75 mm ID and 6.35 mm OD with 99.5% purity, SentroTech). An Inconel wire and quartz rods were fitted within the quartz tube to create annular reactor configurations. $PtSn_x/Al_2O_3$ (nominal 0.5 wt% Pt) was obtained from a toll manufacturer (Riogen), while a $PtMn_x/SiO_2$ catalyst (nominal 2 wt% Pt) was synthesized in-house using the method described by Wu et al[37] through sequential incipient wetness impregnation of pH-adjusted aqueous solutions of manganese (II) nitrate tetrahydrate (Alfa Aesar) and tetraamine platinum (II) nitrate (99.995% trace metals basis, Aldrich) onto

Davisil silica gel (200 – 425 mesh size, grade 643, Aldrich). The sample was dried under ambient conditions, calcined at 550 °C, and then reduced for 30 minutes at 550 °C in a 50 ml/min flow of 10% hydrogen, balance nitrogen. The two platinum-containing catalysts are labeled as "PtMn" and "PtSn," respectively, in the results section. Packed beds of 20 mg of catalyst were loaded upstream of a quartz wool plug situated in the hottest region of the reactor. Inert materials were loaded in the same fashion but were placed both in the hottest region of the reactor and downstream of the heated region during separate tests. "Downstream" or "DS" is added to results to signify this latter sample location where applicable.

The catalysts were characterized via x-ray diffraction (XRD), x-ray fluorescence (XRF), Brunauer Emmett Teller (BET) surface area analysis, and transmission electron microscopy (TEM). XRD analysis determined the crystalline phases present within Pt-based catalysts and was conducted with a Bruker D2 Phaser operating in Bragg-Brentano geometry. XRF elemental composition measurements were taken with an Orbis Micro-XRF using a 30 µm spot size, 20 kV voltage, and 800 µamp current. Surface area measurements were taken with a Micromeritics Gemini 2360 Surface Area Analyzer. Samples were outgassed overnight at 120 °C in flowing nitrogen prior to analysis. A JEOL JEM 2010 F field emission microscope was used for TEM imaging.

Reactors were fitted within a vertically mounted clam-shell furnace with a heated chamber 10 inches in length. During reactions, feed gas was directed downward through the reactor. Temperature was measured with a K-type thermocouple built into the furnace, which was external to the reactor tubes. This external temperature was related to the temperature within the reactor tubes by feeding a K-type thermocouple into the open reactor tubes in one-inch increments under flowing nitrogen to gather temperature profiles prior to ethane reaction. Temperature profiles were used to calculate kinetically averaged residence times for ethane reactant within the open-tube quartz, alumina, and stainless-steel reactors, as is explained in the supporting information. Dehydrogenation of ethane was performed with feed gas compositions of 2.5, 5, 10, and 25% ethane in nitrogen with a total flow of 20 ml/min with furnace temperatures set from 575 – 700 °C in increments of 25 °C and pressure of approximately 0.8 atm (atmospheric pressure in Albuquerque, NM). Effluent gas composition was measured with a Varian CP3800 gas chromatograph equipped with a flame ionization detector (FID) and an Agilent 490 micro GC equipped with a thermal conductivity detector (TCD). Ethane conversion, ethylene selectivity, and ethylene yield were calculated as follows:

$$X_{ethane} = \frac{(C_2H_{6\,in})/N_{2\,in} - (C_2H_{6\,out})/N_{2\,out}}{(C_2H_{6\,in})/N_{2\,in}} * 100\%$$

$$S_{ethylene} = \frac{C_2H_{4\,out}/N_{2\,out}}{(C_2H_{6\,in})/N_{2\,in} - (C_2H_{6\,out})/N_{2\,out}} * 100\%$$

$$Y_{ethylene} = X_{ethane} * S_{ethylene}$$

Area counts generated from the GC FID signal were used to determine ethane and ethylene concentrations entering and exiting the reactors, since these counts are proportional to the concentration of those gaseous species. The nitrogen concentration in the gas flowing in and out of reactor (measured via TCD) was used as an internal standard to correct for the change in total moles of gas that is a result of the dehydrogenation reaction. Since the molar flow rate of N_2 through the reactor remains unchanged, the N_2 counts cancel out of this equation providing a correction for the change in

volume due to reaction. Similarly, the total GC FID area of the detected hydrocarbons allows us to generate a carbon balance as explained in the supporting information. In these experiments, formation of coke was observed only in a few cases, generally when a catalyst was used. Coke formation was measured via several methods. Carbon analysis was conducted on spent Pt catalysts to quantify coke formation using a Costech ECS 4010 Elemental Analyzer. Recovered samples were combusted at 980 °C. Carbon dioxide produced was separated via gas chromatography and detected using a ThermoFisher Scientific Delta V Plus mass spectrometer. Following an isothermal reaction at a furnace temperature of 700 °C for 4 hours in 5% ethane, the quartz tube with and without addition of quartz wool and $PtMn_x$-SiO_2 and $PtSn_x$-Al_2O_3 catalysts was also visually inspected for coke deposits.

Results and Discussion

We first conducted physical characterization of the solids whose reactivity for ethane dehydrogenation was compared to that of an open tube reactor. As measured by XRF, Pt content in PtSn and PtMn catalysts was 0.4 and 1.8 wt%, respectively, which is near the nominal loadings of 0.5 and 2 wt%. Ceria-zirconia contained 6.9 at% zirconium dopant. Composition and surface area for select samples are listed in **Table S1**. TEM images of Pt-containing catalysts show metallic particles several nanometers in diameter (**Figure S1**). Crystalline phases of ceria-zirconia, alumina, and quartz powders were confirmed via XRD analysis (**Figure S2**). Prior to running reactions with these materials, we measured temperature profiles in the quartz, alumina, and stainless-steel reactors while flowing nitrogen through each. The temperatures within each reactor were measured in 1 – inch segments along the 10 – inch heated region of the reactor and were referenced to a thermocouple built into the furnace but external to the reactor. These profiles, which are shown in **Figure S3**, show that the actual temperatures within the open tube reactors were, at highest, approximately 50 °C greater than the temperature recorded by the furnace thermocouple. For simplicity, data listed in this section are presented as a function of the built-in furnace thermocouple temperature.

Ethane dehydrogenation was conducted first using open-tube reactors with 5% ethane feed in nitrogen, 20 ml/min total flow. Results, shown in **Figure 1a**, demonstrate that ethylene yield is influenced by the reactor tube material and that the quartz tube provides the highest yield. Ethane conversion and ethylene selectivity values for the three reactor tubes at the highest tested temperature are shown in **Figure 1b**. Among the three open tube reactors, selectivity to ethylene at the 700 °C operating temperature is relatively similar near 90%, which suggests that the same reaction pathway exists in each. In the absence of a catalyst, reaction within the open tubes is presumed to initiate via thermally-generated methyl free radicals.[24] Ethane conversion, on the other hand, is lower when using the stainless-steel and alumina tubes, leading to the lower ethylene yield. The maximum temperature within each reactor was similar, particularly at the highest set furnace temperature of 700 °C, but there were differences in the temperature profile, with a faster fall off in temperature toward each end of the heated region, Since the reactor inner diameters were not identical, it can result in differing residence time for the gas molecules. Thus, a careful analysis of the residence time was performed by considering the variation in temperature along the axial direction. **Table S2** shows the polynomial fits to the observed temperature profiles in the three different reactor tubes. We calculated the residence time (τ) considering this variation in temperature in the axial direction, assuming uniform radial temperature profiles. We also calculated kinetically averaged residence times (τ_{KA}) based on the work of Fagley.[46]

As explained in the supporting information, we used the term exp(-E_a/RT) as a weighting factor normalized to the average temperature in each reactor which is listed in **Table S3**. The computed residence times at each operating temperature are listed in **Table S4**. Examination of residence times at the highest operating temperature of 700 °C (**Table 1**) suggests that the overall conversion does not directly depend on the residence time, and the tube with the longest residence time does not achieve the highest conversion. This is also true for all other operating temperatures where the reactor operates further from equilibrium. This is because the low flow rate and natural convection in the vertical tube, leads to back mixing. This complex flow pattern implies that the calculated residence time based on plug flow is only an approximation. We therefore suggest that the different performance of the three tubes may be ascribed to differences in surface temperature of the reactor wall, since the reactions are likely initiated in the gas phase in contact with the tube wall. As seen from the measured temperature profiles (**Figure S3**), the alumina and stainless-steel tubes show a more rapid fall off in temperature towards the end of the heated zone, while the quartz tube shows a higher temperature, likely due to differences in thermal conductivity. A complete explanation of the different performance of these tubes will therefore require a CFD model coupled with gas phase kinetics.

Table 1. Computed residence times and conversion at an operating temperature of 700 °C

Reactor tube	ID (mm)	OD (mm)	τ (s)	τ_{KA} (s)	X_{ethane} at 700 °C (%)
Alumina	4.50	6.35	4.02	3.57	68.7
Quartz	4.00	6.00	3.07	2.82	74.5
Quartz (rod)	4.00 (2.00)*	6.00	2.30	2.12	75.1
SS	3.50	6.35	2.40	2.17	51.1

***** Quartz tube reactor (ID 4mm) with an quartz rod (OD 2mm) inserted through the whole length of the heated zone to create an annular flow pattern.

Table 2 lists the concentration of significant gaseous reactants, products, and inerts detected via GC measurement during reactions with the open tube reactors. The raw GC data and the method used for calculating ethane conversion, ethylene selectivity, ethylene yield, and carbon balance are provided in the methods section of the supporting information (**Table S5 – S9**). Methane is the dominant undesired gaseous product of ethane dehydrogenation within each open tube reactor. However, methane remains a very minor product, even at the highest temperatures tested. Molar ratios of H_2/C_2H_4 remain close to unity for the open tube reactors as evident from the concentrations reported in **Table 2**, which confirms the high selectivity toward ethylene and negligible coke formation. These results agree with those in a study by Xu et al, who found similar product distribution trends and H_2/C_2H_4 ratios near unity when conducting ethane pyrolysis in a quartz tube reactor, which held for 50% ethane feed and temperatures higher than those used in this present study.[45] The reported energy barrier for activation of C – H bonds is higher within ethylene than for ethane, which contributes to the selectivity of the thermal dehydrogenation reaction in the absence of an oxidizing agent.[24, 44] Materials like iron and nickel within steel steam cracking coils are known to catalyze coke formation, particularly during start up. Taniewski et al [47] reported decomposition of ethylene within a stainless-steel tube reactor into carbon, methane, and hydrogen during ethane pyrolysis. On the other hand, the authors note the relative stability within a silica reactor. We computed carbon mass balances through gas chromatograph measurements of the gas compositions entering and exiting the reactors, which are

listed in **Table 2** and shown graphically in **Figure S4**. Approximately 95 – 100% of the carbon entering the reactor tubes as ethane is accounted for as methane, ethylene, ethane, propane, and propene exiting each reactor. Previous studies of ethane pyrolysis within inert tube reactors detected additional gaseous products, including acetylene, benzene, 1,3-butadiene, n-butane, toluene, 1-butene, and allene, which we did not detect, likely due to very low concentrations.[48] These hydrocarbons help account for the discrepancy in our carbon balances. The low concentrations of ethane limit the accuracy of TCD measurements, and in our GC analysis using the FID detector, we did not detect hydrocarbons beyond $C_1 – C_3$.

Since the open quartz tube showed the highest yield for ethylene, we next explored whether an annular flow geometry within the quartz tube reactor would be beneficial by changing gas flow dynamics. An annular reactor geometry was accomplished by adding either an Inconel wire or a quartz rod to the center of the open quartz tube. The quartz rod was positioned either within the entire heated region (labeled as "full length") or within the downstream half of the heated region ("half length") of the reactor tube on separate tests. Results are shown in **Figure 1c** and **1d**. Ethylene yield remained highest in the open tube quartz reactor over nearly the whole temperature range tested. At a set temperature of 700 °C, however, the yield is nearly identical in the quartz tube with and without the inclusion of a quartz rod, regardless of rod positioning. Ethylene yield at 700 °C ranged from 66.8 – 66.9% between the open quartz tube with and without inclusion of the annular quartz tube positioned through the entire length of the heated reactor region. The quartz rod inclusion decreased the reactor volume by 25% and changed the effective residence time from 5.10 to 3.83 seconds. The difference in effective residence time caused by varying dimensions between the open quartz, alumina, and stainless-steel reactor tubes is approximately 25% relative to the quartz tube. Because ethylene yield essentially did not change with residence time in the quartz tube reactor configurations, we conclude that the variations in yield between open tube reactor materials could be a result of the different heat transfer characteristics of quartz, alumina, and stainless-steel. Below 675 °C, addition of quartz rods lowered ethylene yield, potentially by slowing heat transfer and leaving the annular quartz rod colder than the quartz tube walls until the furnace temperature and reaction duration increased. Addition of an Inconel wire lowered ethane conversion without significant change to ethylene selectivity, as compared to the open quartz tube. This effect is similar to, but less pronounced, than that of the open stainless-steel tube, which further suggests that heat transfer affects the thermochemical reaction of ethane due to the altered conductivity of metallic components in comparison to ceramic materials such as quartz.

Next, packed beds containing 20 mg of quartz sand, alumina powder, and ceria-zirconia powder were added to the quartz tube reactor. Where specified, the beds were placed downstream of the heated region of the reactor. Otherwise, the beds were positioned in the hottest region. All were supported by a quartz wool plug placed downstream of the bed. These materials are catalytically inert, however, their addition provides significantly more surface area within the reactor, which would be beneficial if the reaction was surface catalyzed. Results are shown in **Figure 1e** and **1f** and in **Table S5**. Addition of each inert component actually had a detrimental effect on ethylene yield over the entire temperature range tested. Ethane conversion was consistently lower with addition of a packed bed to an empty tube. Selectivity was also reduced in the presence of alumina powder due in part to higher methane production. Although an annular quartz rod had little effect on reactor performance at high temperatures, addition of quartz sand lowered performance. The open quartz tube provided an ethane conversion of 74.5% at a set furnace temperature of 700 °C, which decreased to 68.7% when quartz

sand was added downstream of the reactor and to 65.4% when quartz sand was added to the hottest region of the reactor. Addition of these packed bed materials likely alters flow characteristics from open tube and annular configurations. Further, powder addition significantly increases the area of solid surface which may help quench free radical reactions, limiting the extent of ethane conversion. The added solid also changes the void volume in the open tube reactor. We estimate that 8 mg of quartz wool was used to retain the packed bed. At a nominal bulk density of 1g/cc, the occupied volume is 0.028ml. The volume of the quartz reactor is 3.19 ml, hence the added solids have very minimal impact on the residence time of the gas. However, since the added solid is located in the hottest region of the reactor, it leads to lowering the heated volume for the thermal reactions.

We next studied addition of 20 mg packed beds of $PtMn_x - SiO_2$ and $PtSn_x - Al_2O_3$ catalysts (labeled as "PtMn" and "PtSn" for simplicity) to the quartz tube reactor. Catalyst beds were always placed in the hottest region of the reactor. Results are shown in **Figure 1g** and **1h** and in **Table 3**. Here, we find that dehydrogenation performance is highly temperature dependent. At lower temperatures (575 °C), PtMn and PtSn catalysts increased ethane conversion to 42.5% and 35.1%, respectively, compared to 14.5% in the open tube quartz reactor. However, these catalysts degraded as temperature increased, which is evidenced by a decrease in ethylene yield as furnace temperatures increased to 625 °C. Above 625 °C, ethane conversion increased as thermal (as opposed to catalytic) reaction pathways became dominant. At these temperatures, ethylene yield was lower with the Pt-based catalysts than without them. In fact, better yield was achieved at 700 °C with the packed beds of alumina powder and quartz sand than with the catalysts having Pt bimetallics supported on alumina or silica. This suggests that catalytically active materials, like Pt, actually have a negative impact on the thermochemical reaction at elevated temperatures. These active surfaces may be acting as free radical quenchers. To be beneficial, the Pt-based catalysts must be operated at lower temperatures. However, ethane conversion is thermodynamically limited at low temperatures. Higher temperatures appear to deactivate these catalysts. We admit that the catalysts we tested may not have been optimized in terms of the phase and composition, and improved catalysts may lead to stable performance. We also note that the comparison between the catalytic and non-catalytic reaction needs to consider the different volume of active region, since the heated volume of the open tube available for the thermal reaction is much greater than the volume occupied by the catalyst. Hence the residence times for the gas flowing through the catalyst bed is much lower than the residence time for gas flow through the open tube. Nonetheless, these results suggest that the contribution of thermal, gas phase reactions needs to be carefully assessed when developing catalysts for ethane dehydrogenation.

A comparison of performance stability between the catalyzed and non-catalyzed reactor configurations was evaluated by running consecutive reactions using the quartz tube with and without a packed bed of PtMn catalyst. The reaction was run as previously described, while heating from 575 °C to 700 °C. The reactor was cooled to room temperature in flowing nitrogen before performing a second run without any regeneration. **Figure 2** shows the results. The high conversion seen from the PtMn catalyst at low temperature was not seen in the second run. On the other hand, the quartz tube reactor showed stable performance between consecutive runs. TEM analysis of PtMn catalyst in as-prepared and post-reaction (spent) conditions was conducted to determine the cause of deactivation. The high temperatures and reducing conditions generated during non-oxidative dehydrogenation are expected to cause Pt particle sintering. While, some sintering of the PtMn did occur, this effect was surprisingly minor, owing to the

stability imparted through Mn alloying detailed by Wu et al.[31] Mean particle diameter rose from 1.6 to 2.1 nm during the reaction (**Figure S5**), which is not expected to cause catalyst deactivation.

An additional stability test was performed by adding 20 mg of fresh PtMn and PtSn catalysts to the quartz tube reactor, beginning the reaction at 700 °C, and maintaining this temperature for 4 hours. This test was also performed with the open quartz tube alone and the quartz tube with a quartz wool plug added in the same position as used with packed catalyst beds. Results show steady performance from each reactor configuration in terms of yield, conversion, and selectivity (**Figures 3a**, **c**, and **d**). At this temperature, thermal reaction is dominant. Addition of both catalytic and inert materials lowered ethylene yield. Carbon mole balances were calculated by summing the moles of carbon entering and exiting the reactor and correcting for the change in total moles of gas entering and exiting the reactor (**Figure 3b**). Carbon balances are relatively similar between each configuration with values near 95% with the exception of the $PtSn_x - Al_2O_3$ catalyst, which exhibited carbon balance values notably less, near 85%. Experimental limitations in quantifying all the products using the TCD and FID due to low ethane concentrations may contribute to the imperfect carbon balance, since no coke formation was detected with the open quartz tube (**Figure S6c**). We did observe coke deposits on the quartz wool and on both catalysts following the reaction, as shown in **Figure S6 d**,**e**. Carbon analysis yielded 2.5 and 16.4 wt% carbon on spent PtMn and PtSn catalysts, respectively. Therefore coke deposition appears to be a significant cause of Pt catalyst deactivation. Further, this observation implies that material additions to the quartz tube reactor could serve as nucleation sites for coke formation. On the other hand, smooth quartz surfaces free from defects appear to minimize coke formation. To test this hypothesis, the inner walls of a quartz tube reactor were scratched with a stainless-steel wire. Examination of the tube following reaction showed clear signs of carbon deposits (**Figure S6f**). Likewise, a tube that had been used multiple times to support a packed bed showed some carbon deposits on the wall, while a pristine quartz tube showed none. Thus, reactor wall surface roughness may be an important factor which influences carbon deposition during ethane dehydrogenation.

The effect of ethane concentration in feed gas was evaluated while testing the open tube quartz reactor between 575 – 700 °C with 2.5, 5, 10, and 25% ethane in nitrogen while keeping the N_2 flow rate unchanged. At a furnace set temperature of 700 °C in the quartz tube reactor, the ethylene formation rate increases linearly with ethane partial pressure, suggesting the reaction is first order with respect to ethane (**Figure S7**). Sundaram et al similarly found the ethane thermal cracking reaction to be first order.[49] Ethane conversion decreased with higher ethane concentrations, while ethylene selectivity varied only between 86.4 – 89.5% at 700 °C among the different ethane concentrations (**Figure S8**). Likewise, selectivity only varied by several percent among the different ethane concentrations when compared at different reactor temperatures but at similar conversions. These results demonstrate the benefit of quartz tube reactors, which show robust dehydrogenation performance when operating for repeated cycles and with variation in feed gas composition.

Significant study has been dedicated toward the development of catalysts which can withstand demanding conditions involved in ethane dehydrogenation. Often these studies do not distinguish the roles of the catalytic and thermal reactions, which become obscured at high reaction temperatures. Particularly in non-oxidative dehydrogenation studies, dehydrogenation activity may be mistakenly ascribed to the catalyst, whereas thermally induced free radical reactions are actually the dominant pathway. We demonstrate here that high ethylene yield and selectivity are achieved thermally with a simple open tube reactor. Introduction of both catalytic and inert materials into the heated reactor

region was detrimental to the thermal reaction, resulting in lowered yield. Open tube reactors have been studied in the past, usually in the context of the oxidative coupling of methane. In their study of the OCM reaction, Keller and Bhasin[9] found that a stainless steel tube reactor led primarily to the formation of CO_2, but that a quartz tube was completely inert at temperatures ranging from 700 °C to 960 °C. Taniewski et al[47] demonstrated the stability of ethylene in a silica tube reactor at 700 °C and a lower tendency toward coke formation compared to stainless steel reactors. Xu et al. achieved an ethylene yield of 56% with 61.7% conversion and 90.8% selectivity when using an open quartz tube reactor with 50% ethane feed gas.[45] These results are comparable to our observations herein. We further show that preparation of the quartz reactor walls is an important factor in ethylene selectivity. Imperfections in the quartz surface appeared to nucleate coke formation.

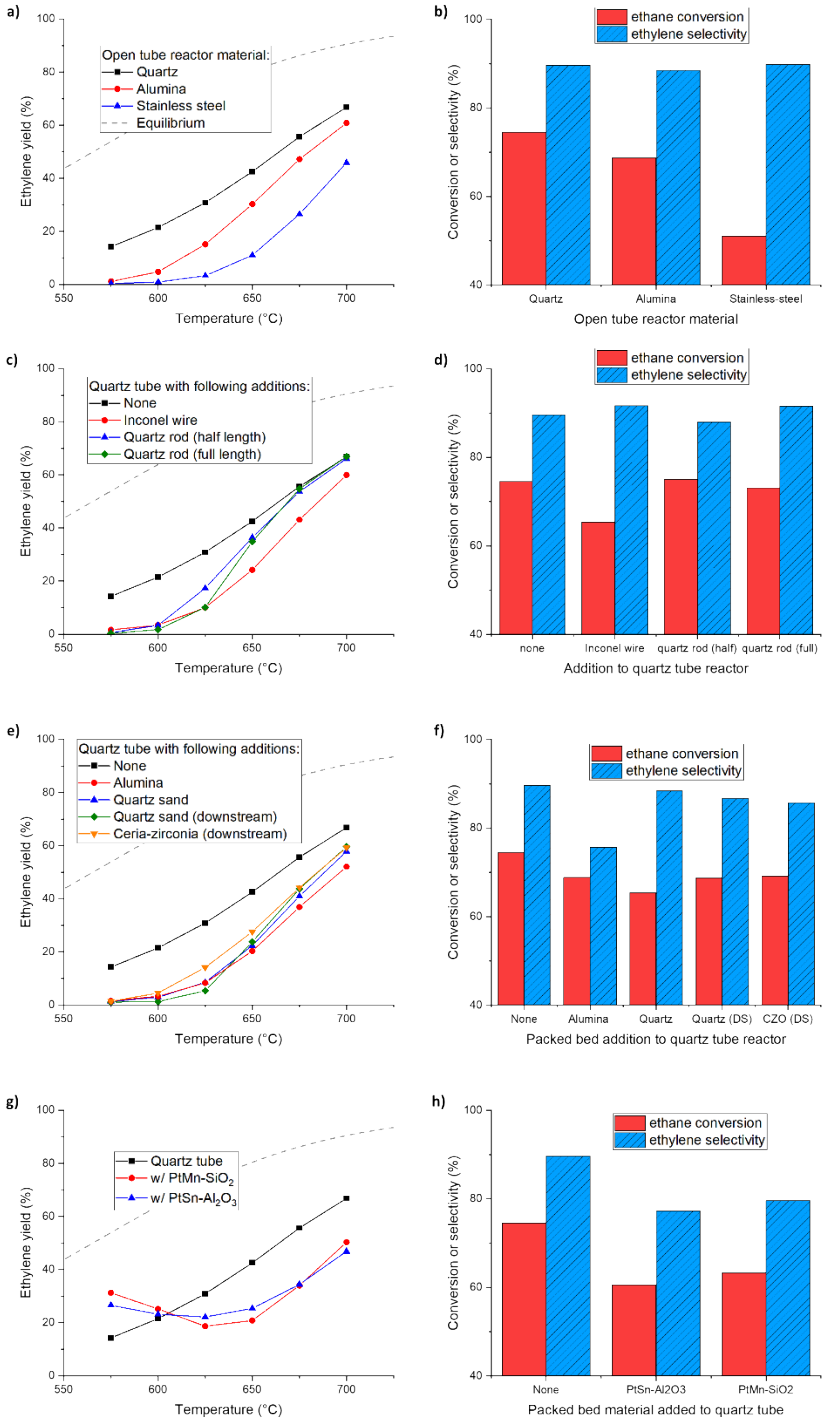

Figure 1. Ethylene yield as a function of temperature for 5% ethane in nitrogen gas fed into (a) open tube reactors, (c) quartz tube reactors with annular Inconel wire and quartz rods placed within the reactor, (e) quartz tube reactors beds of inert material and with annular Inconel wire inclusion, and (e) quartz tube reactors with packed beds of inert material, and (g) quartz tube reactors with packed beds of bimetallic Pt catalysts. Ethylene selectivity and ethane conversions at a temperature of 700 °C for the respective reactor designs (b, d, f, h). The results for other temperatures are shown in Table S5.

Table 2. Gaseous products measured in mole percent as a function of temperature from reaction of 5% ethane feed gas in open tube reactors.

Quartz tube											
Temperature (°C)	**H_2 (mol %)**	**N_2 (mol%)**	**CH_4 (mol %)**	**C_2H_6 (mol %)**	**C_2H_4 (mol %)**	**C_3H_8 (mol %)**	**C_3H_6 (mol %)**	**$X_{C_2H_6}$ (%)**	**$S_{C_2H_4}$ (%)**	**$Y_{C_2H_4}$ (%)**	**C balance (%)**
575	0.47	94.42	0.01	4.37	0.73	0.00	0.00	14.5	98.3	14.2	100
600	0.82	93.94	0.01	4.09	1.13	0.00	0.00	21.9	98.3	21.5	100
625	1.27	93.50	0.02	3.57	1.62	0.00	0.01	32.2	95.8	30.8	99
650	1.90	92.94	0.03	2.91	2.21	0.00	0.01	44.1	96.4	42.5	99
675	2.66	92.29	0.06	2.10	2.87	0.00	0.01	59.4	93.7	55.7	98
700	3.47	91.61	0.11	1.32	3.47	0.00	0.02	74.5	89.7	66.8	95
bypass	0.02	94.48	0.00	5.50	0.00	0.00	0.00	-	-	-	-
Alumina tube											
Temperature (°C)	**H_2**	**N_2**	**CH_4**	**C_2H_6**	**C_2H_4**	**C_3H_8**	**C_3H_6**	**$X_{C_2H_6}$ (%)**	**$S_{C_2H_4}$ (%)**	**$Y_{C_2H_4}$ (%)**	**C balance (%)**
575	0.04	94.61	0.00	5.28	0.06	0.00	0.00	2.6	45.6	1.2	99
600	0.16	94.47	0.00	5.11	0.26	0.00	0.00	6.0	79.0	4.8	99
625	0.54	94.13	0.01	4.50	0.82	0.00	0.00	16.6	91.5	15.1	99
650	1.25	93.42	0.02	3.67	1.64	0.00	0.00	32.2	93.9	30.3	98
675	2.17	92.66	0.04	2.58	2.53	0.00	0.01	51.8	91.1	47.2	96
700	3.12	91.78	0.10	1.69	3.29	0.00	0.02	68.7	88.5	60.8	94
bypass	0.02	94.70	0.00	5.28	0.00	0.00	0.00	-	-	-	-
Stainless steel tube											
Temperature (°C)	**H_2**	**N_2**	**CH_4**	**C_2H_6**	**C_2H_4**	**C_3H_8**	**C_3H_6**	**$X_{C_2H_6}$ (%)**	**$S_{C_2H_4}$ (%)**	**$Y_{C_2H_4}$ (%)**	**C balance (%)**
575	0.11	95.52	0.00	4.35	0.02	0.00	0.00	2.5	13.5	0.3	98
600	0.13	95.38	0.00	4.44	0.04	0.00	0.00	4.0	23.2	0.9	97
625	0.22	95.18	0.00	4.44	0.15	0.00	0.00	5.3	62.3	3.3	98
650	0.50	95.00	0.01	3.99	0.51	0.00	0.00	13.1	84.5	11.0	98
675	1.15	94.19	0.02	3.38	1.26	0.00	0.00	29.0	91.3	26.5	98
700	2.18	93.31	0.04	2.30	2.16	0.00	0.01	51.1	89.9	45.9	96
bypass	0.02	95.02	0.00	4.96	0.00	0.00	0.00	-	-	-	-

Table 3. Gaseous products measured in mole percent as a function of temperature from reaction of 5% ethane feed gas in quartz tube reactors loaded with catalyst beds

$PtSn_x - Al_2O_3$											
Temperature (°C)	**H_2**	**N_2**	**CH_4**	**C_2H_6**	**C_2H_4**	**C_3H_8**	**C_3H_6**	**$X_{C_2H_6}$ (%)**	**$S_{C_2H_4}$ (%)**	**$Y_{C_2H_4}$ (%)**	**C balance (%)**
575	1.58	93.59	0.06	3.38	1.38	0.00	0.00	35.1	75.7	26.6	93
600	1.41	93.63	0.04	3.71	1.22	0.00	0.00	29.3	78.9	23.2	95
625	1.40	93.47	0.04	3.89	1.20	0.00	0.01	28.1	78.8	22.1	95
650	1.58	93.32	0.04	3.66	1.38	0.00	0.00	32.9	77.2	25.4	93

675	2.06	92.89	0.07	3.07	1.90	0.00	0.01	44.5	77.3	34.4	91
700	2.80	92.24	0.12	2.21	2.63	0.00	0.01	60.6	77.3	46.8	89
bypass	0.02	94.97	0.00	5.01	0.00	0.00	0.00	-	-	-	-
$PtMn_x - SiO_2$											
Temperature (°C)	**H_2**	**N_2**	**CH_4**	**C_2H_6**	**C_2H_4**	**C_3H_8**	**C_3H_6**	**$X_{C_2H_6}$ (%)**	**$S_{C_2H_4}$ (%)**	**$Y_{C_2H_4}$ (%)**	**C balance (%)**
575	2.07	93.23	0.03	3.03	1.65	0.00	0.00	42.5	73.6	31.2	89
600	1.57	93.49	0.02	3.56	1.37	0.00	0.00	34.7	72.5	25.2	91
625	1.14	93.69	0.01	4.10	1.05	0.00	0.00	27.1	68.9	18.7	92
650	1.29	93.56	0.02	3.96	1.17	0.00	0.00	29.5	70.4	20.8	92
675	2.02	92.90	0.05	3.13	1.89	0.00	0.01	43.8	77.5	34.0	91
700	3.03	91.89	0.10	2.09	2.87	0.00	0.01	63.2	79.5	50.3	89
bypass	0.02	94.75	0.00	5.23	0.00	0.00	0.00	-	-	-	-

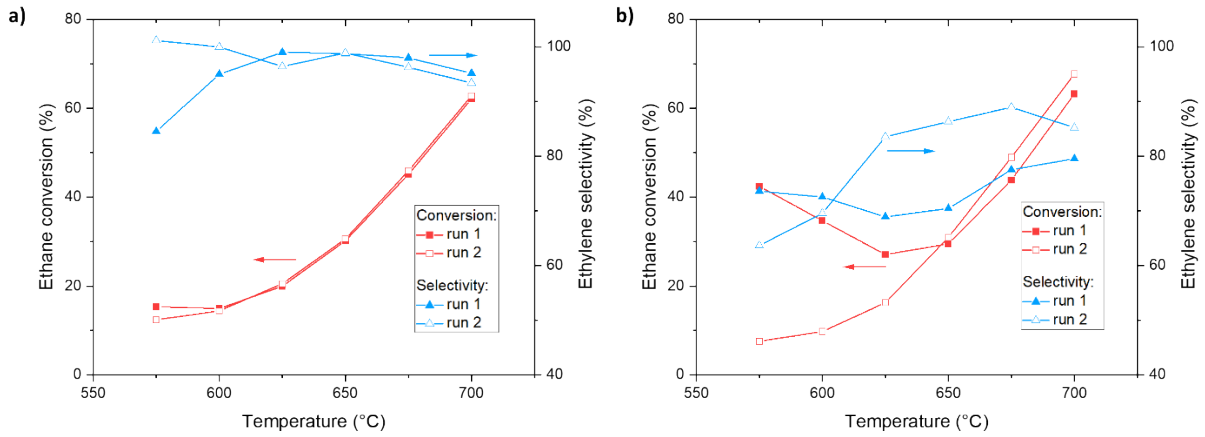

Figure 2. Performance through two consecutive dehydrogenation runs using 5% ethane feed gas with (a) an open quartz tube reactor and (b) a quartz tube reactor loaded with 20 mg of PtMn catalyst.

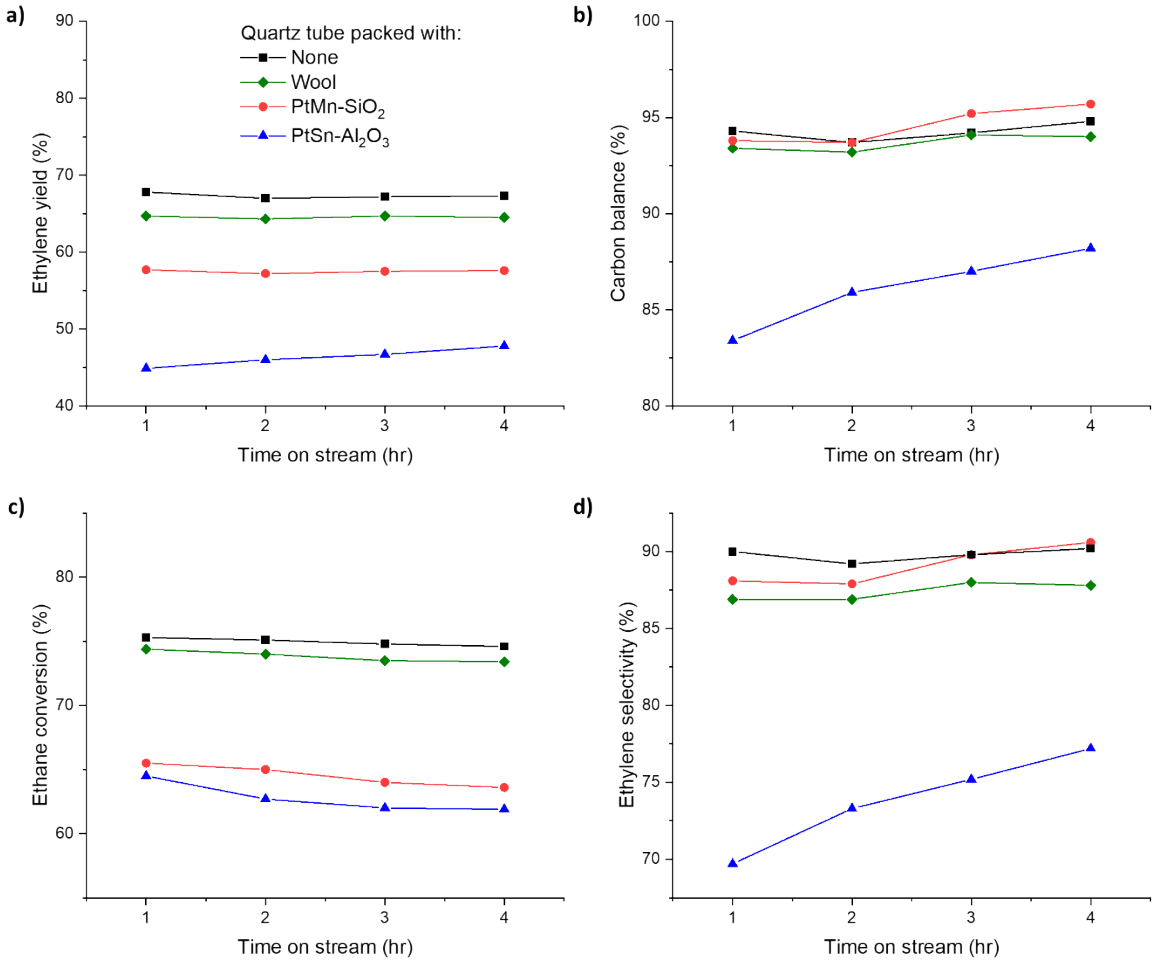

Figure 3. Dehydrogenation performance of a quartz tube reactor with and without addition of quartz wool and Pt-based catalysts held at a furnace temperature of 700 °C in terms of (a) ethylene yield, (b) carbon balance, (c) ethane conversion, and (d) ethylene selectivity.

Conclusions

The results indicate that thermal, gas phase reactions dominate the ethane dehydrogenation reaction performed at high temperature (700 °C). With the single zone tube furnace used in this work, the temperature varies both axially and radially in a wall heated reactor. Hence we used the temperature indicated by the furnace controller to report the effect of temperature. A quartz tube that was pristine and free of defects led to superior performance compared to a reactor containing inert solids or even state of the art Pt-based catalysts. At elevated temperatures, Pt-based catalysts showed rapid deactivation due to coke deposition and some sintering. In contrast, the open tube continued to perform with no apparent deactivation and minimal coke formation. The role of the gas flow and temperature profile merits further study, since our experiments were performed at low flow rates where natural convection leads to a complex flow pattern and with gas residence times up to 4s. This

work suggests that future research be focused on optimizing the reactor geometry to achieve better heat integration and to quench any undesirable free radical reactions. Such modular reactor designs may be suitable for conversion of distributed ethane resources available through fracking. Fracking-derived natural gas typically contains ethane concentrations ranging between 0 – 25%, as were used in this study. Regardless of ethane concentration, the open tube quartz reactor consistently out-performed packed bed reactors in our work. However, we recognize that a comparison of the volumetric productivity of the thermal and the catalytic reactions needs to consider the much larger heated volume in the open tube compared to the volume occupied by the catalyst. We observed that the presence of any solid within the reactor, even an active catalyst, had a negative effect on overall ethylene yield at the highest temperatures of operation. Thus, quartz represents a viable reactor material that does not cause significant coking or suffer from carburization-induced degradation as seen in conventional steam cracking furnaces.

Acknowledgements

This material is based upon work supported by the U.S. Department of Energy's Advanced Manufacturing Office, award number DE-LC 000L059. This work was performed, in part, at the Center for Integrated Nanotechnologies, an Office of Science User Facility operated for the U.S. Department of Energy (DOE) Office of Science. Sandia National Laboratories is a multimission laboratory managed and operated by National Technology & Engineering Solutions of Sandia, LLC, a wholly owned subsidiary of Honeywell International, Inc., for the U.S. DOE's National Nuclear Security Administration under contract DE-NA-0003525. The views expressed in the article do not necessarily represent the views of the U.S. DOE or the United States Government. Catalyst synthesis and characterization was supported by the NSF/ERC CISTAR, which is supported by the National Science Foundation under Cooperative Agreement No. EEC-164772.

References

[1] I. Amghizar, L.A. Vandewalle, K.M.V. Geem, G.B. Marin, New Trends in Olefin Production, Engineering, (2017) 171-178.
[2] T. Ren, M.K. Patel, K. Blok, Steam cracking and methane to olefins: Energy use, CO_2 emissions and production costs, Energy, 33 (2008) 817-833.
[3] M.N. Rosli, N. Aziz, Simulation of ethane steam cracking with severity evaluation, IOP Conf. Ser.: Mater. Sci. Eng, 162 (2017).
[4] E.E. Stangland, Shale Gas Implecations for C_2-C_3 Olefin Production: Incumbent and Future Technology, Annu. Rev. Chem. Biomol. Eng., 9 (2018) 341-364.
[5] S.H. Symoens, N. Olahova, A.E. Muñoz Gandarillas, H. Karimi, M.R. Djokic, M.-F. Reyniers, G.B. Marin, K.M. Van Geem, State-of-the-art of Coke Formation during Steam Cracking: Anti-Coking Surface Technologies, Ind. Eng. Chem. Res., 57 (2018) 16117-16136.
[6] X. Li, S. Liu, H. Chen, S.-z. Luo, F. Jing, W. Chu, Improved Catalytic Performance of Ethane Dehydrogenation in the Presence of CO2 over Zr-Promoted Cr/SiO2, ACS Omega, 4 (2019) 22562-22573.
[7] S.A. Theofanidis, C. Loizidis, E. Heracleous, A.A. Lemonidou, CO2-oxidative ethane dehydrogenation over highly efficient carbon-resistant Fe-catalysts, J. Catal., 388 (2020) 52-65.

[8] Y. Cheng, L. Zhou, J. Xu, C. Miao, W. Hua, Y. Yue, Z. Gao, Chromium-based catalysts for ethane dehydrogenation: Effect of SBA-15 support, 2016, 234 (2016) 370-376.
[9] G.E. Keller, M.M. Bhasin, Synthesis of Ethylene via Oxidative Coupling of Methane, Journal of Catalysis, 73 (1982) 9-19.
[10] A. Al-Mamoori, S. Lawson, A.A. Rownaghi, F. Rezaei, Oxidative dehydrogenation of ethane to ethylene in an integrated CO_2 capture-utilization process, Appl. Catal. B, 278 (2020).
[11] H. Seki, H. Saito, K. Toko, Y. Hosono, T. Higo, J.G. Seo, S. Maeda, K. Hashimoto, S. Ogo, Y. Sekine, Effect of Ba addition to Ga-α-Al_2O_3 catalyst on structure and catalytic selectivity for dehydrogenation of ethane, Applied Catalysis A, General, 581 (2019) 23-30.
[12] W. Ding, K. Zhao, S. Jiang, Z. Zhao, Y. Cao, F. He, Alkali-metal enhanced $LaMnO_3$ perovskite oxides for chemical looping oxidative dehydrogenation of ethane, Applied Catalysis A, General, 609 (2021).
[13] A.M. Gaffney, O.M. Mason, Ethylene production via Oxidative Dehydrogenation of Ethane using M1 catalyst, Catal. Today, 285 (2017) 159-165.
[14] S. Wang, K. Murata, T. Hayakawa, S. Hamakawa, K. Suzuki, Oxidative Dehydrogenation of Ethane Over Zirconia-Supported Lithium Chloride Catalysts, Chem Eng Technol, 23 (2000) 1099-1103.
[15] A.S. Al-Awadi, S.M. Al-Zahrani, A.M. El-Toni, A.E. Abasaeed, Dehydrogenation of Ethane to Ethylene by CO_2 over Highly Dispersed Cr on Large-Pore Mesoporous Silica Catalysts, Catalysts, 10 (2020).
[16] C.P. Kumar, S. Gaab, T.E. Muller, J.A. Lercher, Oxidative Dehydrogenation of Light Alkanes on Supported Molten Alkali Metal Chloride Catalysts, Top Catal, 50 (2008) 156-167.
[17] Y. Gao, X. Wang, J. Liu, C. Huang, K. Zhao, Z. Zhao, X. Wang, F. Li, A molten carbonate shell modified perovskite redox catalyst for anaerobic oxidative dehydrogenation of ethane, Science Advances, 6 (202).
[18] A. Talati, M. Haghighi, F. Rahmani, Oxidative dehydrogenation of ethane to ethylene by carbon dioxide over Cr/TiO2-ZrO2 nanocatalyst: Effect of active phase and support composition on catalytic properties and performance, Advanced Powder Technology, 27 (2016) 1195-1206.
[19] M.L. Rodriguez, D.E. Ardissone, E. Lopez, M.N. Pedernera, D.O. Borio, Reactor Designs for Ethylene Production via Ethane Oxidative Dehydrogenation: Comparision of Performance, I&EC Research, 50 (2010) 2690-2697.
[20] Y.S. Al-Zeghayer, S.I.A.-. Mayan, T.A. Al-Smari, Oxidative Dehydrogenation of Ethane to Ethylene Over Mo-V-Nb Catalysts: Effect of Calcination Temperature and Type of Support, Engineering Science, 22 (2010) 21-28.
[21] Y.S. Yun, M. Lee, J. Sung, D. Yun, T.Y. Kim, H. Park, K.R. Lee, C.K. Song, Y. Kim, J. Lee, Y.-J. Seo, I.K. Song, J. Yi, Promoting effect of cerium on MoVTeNb mixed oxide catalyst for oxidative dehydrogenation of ethane to ethylene, Appl. Catal. B, 237 (2018).
[22] D. Melzer, G. Mestl, K. Wanninger, Y. Zhu, N.D. Browning, M. Sanchez-Sanchez, J.A. Lercher, Design and synthesis of highly active MoVTeNb-oxides for ethane oxidative dehydrogenation, Nature Communications, (2019).
[23] K. Takanabe, S. Shahid, Dehydrogenation of Ethane to Ethylene via Radical Pathways Enhanced by Alkali Metal Based Catalyst in Oxysteam Condition, AIChE, 63 (2016) 105-110.
[24] E. Heracleous, A.A. Lemonidou, Homogeneous and heterogeneous pathways of ethane oxidative and non-oxidative dehydrogenation studied by temperature-programmed reaction, Applied Catalysis A: General, 269 (2004) 123-135.
[25] C. Xin, F. Wang, G.Q. Xu, Tuning surface V^{5+} concentration in M1 phase $MoVSbO_x$ catalysts for ethylene production from ethane through oxidative dehydrogenation reaction, Applied Catalysis A, General, 610 (2021).
[26] Z. Yang, H. Li, H. Zhou, L. Wang, L. Wang, Q. Zhu, J. Xiao, X. Meng, J. Chen, F.-S. Xiao, Coking-Resistant Iron Catalyst in Ethane Dehydrogenation Achieved through Siliceous Zeolite Modulation, JACS, (2020).

[27] L.-C. Wang, Y. Zhang, J. Xu, W. Diao, S. Karakalos, B. Liu, X. Song, W. Wu, T. He, D. Ding, Non-oxidative dehydrogenation of ethane to ethylene over ZSM-5 zeolite supported iron catalysts, Applied Catalysis B: Environmental, 256 (2019).
[28] M.H. Jeong, J. Sun, G.Y. Han, D.H. Lee, J.W. Bae, Successive reduction-oxidation activity of FeO_x/TiO_2 for dehydrogenation of ethane and subsequent CO_2 activation, Appl. Catal. B, 270 (2020).
[29] S. Yusuf, V. Haribal, D. Jackson, L. Neal, F. Li, Mixed iron-manganese oxides as redox catalysts for chemical looping-oxidative dehydrogenation of ethane with tailorable heat of reactions, Appl. Catal. B, 257 (2019).
[30] J.J.H.B. Sattler, J. Ruiz-Martinez, E. Santillan-Jimenez, B.M. Weckhuysen, Catalytic Dehydrogenation of Light Alkane on Metals and Metal Oxides, Chemical Reviews 114 (2014) 10613-10653.
[31] Z. Wu, B.C. Bukowski, Z. Li, C. Milligan, L. Zhou, T. Ma, Y. Wu, Y. Ren, F.H. Ribeiro, N. Delgass, J. Greeley, G. Zhang, J.T. Miller, Changes in Catalytic and Adsorptive Properties of 2 nm Pt_3Mn Nanoparticles by Subsurface Atoms, JACS, 140 (2018) 14870-14877.
[32] E.C. Wegener, Z. Wu, H.-T. Tseng, J.R. Gallagher, Y. Ren, R.E. Diaz, F.H. Ribeiro, J.T. Miller, Structure and reactivity of Pt-In intermetallic alloy nanoparticles: Highly selective catalysts for ethane dehydrogenation, Catalysis Today, 299 (2018) 146-153.
[33] Q. Zhang, K. Zhang, S. Zhang, Q. Liu, L. Chen, X. Li, C. Wang, L. Ma, Ga^{3+}-stabilized Pt in PtSn-Mg(Ga)(Al)O catalyst for promoting ethane dehydrogenation, Journal of Catalysis, 368 (2018) 79-88.
[34] V.J. Cybulskis, B.C. Bukowski, H.-T. Tseng, J.R. Gallagher, Z. Wu, E. Wegener, A.J. Kropf, B. Ravel, F.H. Ribeiro, J. Greeley, J.T. Miller, Zinc Promotion of Platinum for Catalytic Light Alkane Dehydrogenation: Insights into Geometric and Electronic Effects, ACS Catalysis, 7 (2016) 4173-4181.
[35] Z. Yu, J.A. Sawada, W. An, S.M. Kuznicki, PtZn-ETS-2: A Novel Catalyst for Ethane Dehydrogenation, AIChE, 61 (2015) 4367-4376.
[36] V. Galvita, G. Siddiqi, P. Sun, A.T. Bell, Ethane dehydrogenation on Pt/Mg(Al)O and PtSn/Mg(Al)O catalysts, Journal of Catalysis, 271 (2010) 209-219.
[37] Z. Wu, B.C. Bukowski, Z. Li, C. Milligan, L. Zhou, T. Ma, Y. Wu, Y. Ren, F.H. Ribeiro, W.N. Delgass, J. Greeley, G. Zhang, J.T. Miller, Changes in Catalytic and Adsorptive Properties of 2 nm Pt3Mn Nanoparticles by Subsurface Atoms, J. Am. Chem. Soc., 140 (2018) 14870-14877.
[38] E. Gobina, K. Hou, R. Hughes, Ethane Dehydrogenation in a Catalytic Membrane Reactor Coupled with a Reactive Sweep Gas, Chemical Engineering Science 50 (1995) 2311-2319.
[39] S. Dangwal, R. Liu, S.-J. Kim, High-temperature ethane dehydrogenation in microporous zeolite membrane reactor: Effect of operating conditions, Chem. Eng. J. (Lausanne), 328 (2017) 862-872.
[40] A.M. Avila, Z. Yu, S. Fazli, J.A. Sawada, S.M. Kuznicki, Hydrogen-selective natural mordenite in a membrane reactor for ethane dehydrogenation, Microporous and Mesoporous Materials, 190 (2014) 301-308.
[41] A.M. Champagnie, T.T. Tsotsis, R.G. Minet, E. Wagner, The Study of Ethane Dehydrogenation in a Catalytic Membrane Reactor, Journal of Catalysis, 134 (1991) 713-730.
[42] C.J. Liu, X.D. Chen, T. Chen, X.M. Lian, J.F. Sun, Phas Transformation of Nb in Carburized Zone of 25Cr35NiNb+MA Alloy after Service, Procedia Engineering, 130 (2015) 693-700.
[43] S.A. Sarris, S.H. Symoens, N. Olahova, M.-F. Reyniers, G.B. Marin, K.M.V. Geem, Alumina-based Coating for Coke Reduction in Steam Crackers, Materials, 13 (2020).
[44] A.M. Dean, Predictions of pressure and temperature effects upon radical addition and recombination reactions, The Journal of Physical Chemistry, 89 (1985) 4600-4608.
[45] C. Xu, A.S.A. Shoaibi, C. Wang, H.-H. Carstensen, A.M. Dean, Kinetic Modeling of Ethane Pyrolysis at High Conversion, The Journal of Physical Chemistry A, 115 (2011) 10470-10490.
[46] J.C. Fagley, Simulation of Transport in Laminar, Tubular Reactors and Application to Ethane Pyrolysis, Ind. Eng. Chem. Res., 31 (1992) 58-69.

[47] M. Taniewski, K. Skutil, R. Lachowicz, A. Lachowicz, B. Dudek, D. Czechowicz, Transformations of the products of methane oxidative coupling in the post-catalytic zone of the convertor, Catalysis Today, 13 (1992) 529-536.
[48] M.H. Saldana, G.E. Borgin, K. Wang, A.M. Dean, Comparative Kinetic Analysis of Ethane Pyrolysis at 0.1 and 2.0 MPa, Energy & Fuels, 30 (2016) 9703-9711.
[49] K.M.V.D. Sundaram, P. S.; Froment, G. F., Coke Deposition in the Thermal Cracking of Ethane, AIChE Journal, 27 (1981).